



ACADEMIC  
PRESS

Available online at [www.sciencedirect.com](http://www.sciencedirect.com)

SCIENCE @ DIRECT®

Journal of Solid State Chemistry 176 (2003) 294–305

JOURNAL OF  
SOLID STATE  
CHEMISTRY

<http://elsevier.com/locate/jssc>

# *d*-Electron mediated $4f^7-4f^7$ exchange in Gd-rich compounds; spin density functional study of $Gd_2Cl_3$

Lindsay Roy and Timothy Hughbanks\*

Department of Chemistry, Texas A&M University, P.O. Box 30012, College Station, TX 77842-3012, USA

Received 30 January 2003; accepted 25 March 2003

## Abstract

Spin-density functional theory (SDFT) calculations of the *d*-*f* exchange coupling for the pseudo-one-dimensional (pseudo-1-D) chain compound  $Gd_2Cl_3$  has been carried out using the 1-D model,  $Gd_8Cl_{12}(OPH_3)_4$ , by considering seven variations in the ordering of the  $4f^7$  moments. The calculations indicate that this semiconducting system should exhibit antiferromagnetic ordering of the  $4f^7$  moments in a pattern consistent with published neutron diffraction data. An attempt to account for the calculated magnetic energies of spin patterns using an Ising model was unsuccessful, indicating that the latter model is inappropriate. The qualitative features can be interpreted using a perturbative molecular orbital model that focuses on the influence of the  $4f^7-d$  exchange interaction on the *d*-based molecular orbitals. Fundamental to the *d*-electron-mediated exchange mechanism is the intra-atomic  $4f^7-d$  exchange interaction. The essence of this interaction is present in the Gd atom [ $4f^7 5d^1 6s^2$ ], which is computationally investigated within SDFT. In  $Gd_2Cl_3$ , the *d*-electron-mediated *f*-*f* exchange interaction was interpreted using basic perturbation theory. Computed density of states and spin polarization information was used to support the perturbation-theoretic analysis.

© 2003 Elsevier Inc. All rights reserved.

**Keywords:** DFT; Metal-rich compounds; Broken symmetry approach; Band calculations; Rare-earth magnetism

## 1. Introduction

Experimentalists investigating magnetic materials clearly need theoretical tools that are capable of supplying at least semiquantitative descriptions of magnetically coupled systems so that empirical data can be organized and fitted to appropriate physical models [1]. In addition, qualitative understanding of magnetic exchange in the many different kinds of such coupled systems is imperative for the design of novel inorganic materials with specific magnetic properties.

Researchers have been able to determine the strength and nature of coupling between magnetic centers by gathering data from various experimental sources, including magnetic susceptibility, spin-polarized neutron diffraction, and inelastic neutron scattering [2]. More recently, many have applied modern computational techniques to correlate geometric and electronic structure in efforts to elucidate general trends concerning the strength of magnetic exchange. The electronic

structures of complex solid-state materials have been extensively studied at the tight-binding (e.g., extended Hückel) level and such treatments can provide a qualitative description of magnetic exchange within a proper interpretive scheme [3–5]. Recently, more quantitative descriptions are moving within reach of many magnetochemists using methods based on density functional theory (DFT) and the broken-symmetry approach, which provide reasonable estimates for the exchange coupling constants for a variety of compounds [1,6–9].

A common theoretical/computational method of determining the strength of exchange is based on a spin-dimer analysis of the extended solid [3]. In this approach, one constructs truncated model dimers, and results from the computational studies are used to supply the pairwise-coupling parameters in model Hamiltonians (e.g., Heisenberg or Ising) describing the magnetic properties of the solid. Even if the quantum mechanical method is adequate to tackle this task, several issues arise in evaluating the approach, namely the appropriateness of the selected model Hamiltonian and the possible uncertainty introduced from structural

\*Corresponding author. Fax: +1-979-847-8860.

E-mail address: [trh@mail.chem.tamu.edu](mailto:trh@mail.chem.tamu.edu) (T. Hughbanks).

truncation into the computed parameters. Can the magnetic coupling energy of the solid really be expressed as a sum of pairwise-additive effective exchange interaction energies? If the comparison of experimental data to theory only relies on magnetic susceptibilities, how much confidence can we have in a semiempirical spin-dimer treatment that may include scaling the magnitude of all the exchange parameters as part of the treatment?

Our interest lies in Gd-rich systems (clusters and solids) where Gd magnetic moments are subject to significant interatomic exchange coupling. Of the elements that produce magnetic materials, open-4*f*-shell rare-earth elements provide one of the richest regions for interesting and useful magnetic and conducting properties. However, efforts to understand the relationship between structure and magnetic properties of rare-earth magnetic materials have been hindered because of the complex nature of their magnetic interactions. Difficulties in understanding the key factors controlling magnetic properties are an obstacle to further rational experimental development of this field. Hence, there exists a need for chemically useful yet physically realistic localized bonding schemes that can serve to interpret and predict magnetic behavior in polynuclear lanthanide molecules. The task of building theoretical models for application to rare-earth compounds that are of general applicability, analogous to the Goodenough [10] rules, or the Hay–Thibeault–Hoffmann [11] and Kahn–Briat [12] models, has been challenging.

In efforts to understand the nature of magnetic behavior in rare-earth-rich systems, we have conducted molecular orbital and band structure calculations where the energies and orbitals of such systems are compared as we variably impose ordering patterns of the 4*f*<sup>7</sup> spins. In a previous paper, we treated a molecular model system, [(Gd<sub>3</sub>I<sub>6</sub>)(OPH<sub>3</sub>)<sub>6</sub>]<sup>*n*+</sup> (*n* = 1, 2, 3) and focused on the manner in which metal–metal bonding 5*d* electrons mediate the coupling of 4*f* electrons [13]. In conventional molecular chemistry, mono- and polynuclear Gd complexes contain the metal in the 3+ oxidation state, corresponding to the [(Gd<sub>3</sub>I<sub>6</sub>)(OPH<sub>3</sub>)<sub>6</sub>]<sup>3+</sup> ion. Our treatment focused on the case where *n* = 2 or 1, where one or two electrons, respectively, are involved in Gd–Gd bonding.

In this paper, our focus is on magnetic ordering in the pseudo-one-dimensional (pseudo-1-D) chain compound, Gd<sub>2</sub>Cl<sub>3</sub> [14]. We have performed several spin-density functional theory (SDFT) band structure calculations on a 1-D model for this system in which we have considered a number of variations in the ordering patterns of the 4*f*<sup>7</sup> spins, including a ferromagnetic pattern (maximum magnetization), one “ferrimagnetic” pattern (intermediate magnetization), and several anti-ferromagnetic patterns (zero total magnetization). The energy of each such spin-ordering pattern can be

evaluated simply within an Ising-like model, and Heisenberg exchange parameters can then be inferred.

Because a neutron diffraction study has been conducted on Gd<sub>2</sub>Cl<sub>3</sub> [15], this system offers us an important benchmark for testing the use of the broken-symmetry SDFT method for evaluating magnetic coupling in Gd-rich compounds. The use of SDFT band structure calculations frees us from uncertainties inherent to the spin-dimer approach mentioned in the introductory remarks above. As we shall see, these calculations also shed light on the question of whether magnetic coupling should be described in terms of pairwise interactions in reduced Gd-rich compounds.

## 2. Theoretical background

Exchange interactions between two paramagnetic centers are phenomenologically described using the Heisenberg–Dirac–Van Vleck (HDVV) spin Hamiltonian [16–18]

$$\hat{H} = -J_{ij}\hat{S}_i\hat{S}_j, \quad (1)$$

where  $J_{ij}$  is the magnetic coupling constant describing the spin exchange between different spin states and  $\hat{S}_i$  and  $\hat{S}_j$  are the total spin operators for atoms *i* and *j*. The sign of the magnetic coupling constant is such that  $J_{ij}$  is positive for ferromagnetic coupling and negative for an antiferromagnetic interaction.

In the simplest example of a magnetically coupled system, a dimer where  $S_1 = S_2 = \frac{1}{2}$ , the four basis spin determinants are  $|\alpha\alpha\rangle$ ,  $|\beta\beta\rangle$ ,  $|\alpha\beta\rangle$ , and  $|\beta\alpha\rangle$ . Since  $\hat{H}$ , the total spin operator  $\hat{S}^2$ , and the *z*-component of the spin operator,  $\hat{S}_z$ , commute, it is possible to determine a set of eigenfunctions relating all three operators. The eigenfunctions of  $\hat{S}^2$  and  $\hat{S}_z$  are denoted as  $|S, M_s\rangle$  and it is straightforward to show that  $|1, 1\rangle = |\alpha, \alpha\rangle$  and  $|1, -1\rangle = |\beta, \beta\rangle$ , whereas determinants  $|0, 0\rangle$  and  $|1, 0\rangle$  consist of a linear combination of  $|\alpha, \beta\rangle$  and  $|\beta, \alpha\rangle$ . The coupling constant may then be obtained as the energy difference between the singlet and triplet states.

In extended systems, all possible pairwise interactions are considered, yielding the HDVV spin Hamiltonian

$$\hat{H} = - \sum_{i < j} J_{ij} \hat{S}_i \hat{S}_j; \quad (2)$$

the summations usually include only neighbors (*i* and *j*) that are in proximity to each other. In many cases, it is difficult or impossible to find the eigenfunctions of the HDVV spin Hamiltonian. A common alternative for computation of the magnetic coupling constant is to make use of the simpler Ising Hamiltonian ( $\hat{H}^I$ ) [19–21], where the total spin operators are replaced by their *z*-components:

$$\hat{H}^I = - \sum_{i < j} J'_{ij} \hat{S}_{z,i} \hat{S}_{z,j}. \quad (3)$$

$J_{ij}^{\prime}$  values are calculated directly from energy differences between the states of maximum and minimum  $M_S$ , the so-called “ferromagnetically coupled” and “antiferromagnetically coupled” states, respectively. In the Ising Hamiltonian, it is common to assign eigenvalues of  $+1$  ( $\alpha$ ) and  $-1$  ( $\beta$ ) to the “pseudo-spin”, so that the magnitudes of the Ising and Heisenberg coupling constants differ by quantities on the order of  $\hat{S}_i \hat{S}_j$ . Eigenfunctions of  $\hat{H}^I$  are not generally eigenfunctions of  $\hat{S}^2$ , but are eigenfunctions of  $\hat{S}_z$ , making it possible to use  $M_S$  as a quantum number. Considering again our previous example where  $S_1 = S_2 = \frac{1}{2}$ , a pure ( $M_S = 1$ ) component of the ferromagnetic state is explicitly described as the determinant  $|\alpha\alpha\rangle$  since it is a spin eigenfunction. In contrast, the antiferromagnetic state cannot be described because there are two determinants with  $M_S = 0$  ( $|\alpha\beta\rangle$  and  $|\beta\alpha\rangle$ ) and neither is an eigenfunction of the total spin operator  $\hat{S}^2$ .

The Ising Hamiltonian can be connected to all the unrestricted formalisms based on the single-determinant approach of SDFT via the broken-symmetry approach. The single-determinantal nature of SDFT poses problems because it does not allow the calculation of a pure spin eigenfunction. As in the treatment using the Ising Hamiltonian, the single-determinant description of the high-spin states is straightforward (because high-spin states are eigenfunctions of  $\hat{S}^2$  and  $\hat{S}_z$  and therefore suffer no spin contamination). However, calculation of the pure low-spin state is not possible and one is forced to use a broken-symmetry approach which allows one to calculate spin-state energy differences using the results of a single-determinantal function [22,23]. Dai and Whangbo recently explored the relationship of the spin-dimer approach using broken-symmetry Heisenberg Hamiltonian and the magnetic solid approach using the Ising Hamiltonian [24]. They showed that a description of the spin-exchange interactions of a magnetic solid treated with a Heisenberg spin Hamiltonian can be extracted from broken-symmetry SDFT calculations that are most directly consistent with the Ising spin Hamiltonian. In our results, we have employed a broken-symmetry approach to evaluate the magnetic coupling constants between Gd centers.

### 3. Broken-symmetry approach in gadolinium compounds

The  $5d$  and  $6s$  valence orbitals of lanthanide atoms are diffuse, but in an important sense the  $4f$  electrons are essentially core electrons—in highly contracted orbitals that preclude appreciable overlap with neighboring atoms [25]. Because such  $4f$  overlaps are so small, superexchange coupling (mediated by overlap with intervening ligand orbitals) between nearby lanthanide centers is largely precluded. Because of their core-like radial extension, lanthanide  $4f$  electrons should not

be viewed as typical “band electrons”. In rare-earth intermetallic compounds, an indirect pathway involving the localized  $4f$  electrons and the conduction band electrons is responsible for magnetic ordering. When the conduction electrons are spin-polarized, as in Fe- or Co-rich compounds (e.g.,  $\text{Nd}_2\text{Fe}_{14}\text{B}$  and  $\text{SmCo}_5$  and other related permanent magnets), the exchange coupling to the conduction electrons can be significant. Elemental gadolinium is a metallic ferromagnet with an ordering temperature just above room temperature. Within the bulk metal, stabilizing  $4f$ – $5d$  exchange induces some spin polarization of  $5d$  electrons in the vicinity of the Fermi level that cooperatively aligns the  $4f$  moments [26]. This indirect exchange mechanism, which was originally treated in magnetically dilute systems (RKKY exchange) [27–29], produces an *effective*  $4f$ – $4f$  coupling and is responsible for the observed magnetic properties.

Of course, in any real system where one might have a single  $f$  electron on adjacent lanthanide centers (e.g., a bimetallic cerium complex), spin-orbit coupling within the  $4f$ -shell would have to be accounted for in addition to interatomic  $f$ – $f$  exchange. Thus, for handling interatomic spin-exchange interactions in the rare-earth elements, gadolinium offers the least complicated starting point. For its ground configuration,  $[\text{Xe}]4f^7 5d^1 6s^2$ , the ground state and lowest excited states are derived by coupling the  $5d$  electron ( $^2D$ ) with the  $^8S$  state of the  $4f^7$  core to give a  $^9D$  ground state and an excited  $^7D$  state. Loosely speaking, these states respectively correspond to the  $d$ -electron spin either aligning with or against the exchange-coupled spins of the  $f^7$  core. The results of SDFT calculation of the atom are discussed below. In this paper, we concern ourselves entirely with systems containing  $4f^7$  gadolinium centers, where spin-orbit coupling effects are absent in first order (for the  $^8S$  state of the  $4f^7$  core) and can therefore be safely neglected.

Our treatment of coupled Gd centers generalizes the symmetry-broken approach. For two Gd centers, SDFT can be used to calculate the energy of  $|\uparrow_7, \uparrow_7\rangle$  and  $|\uparrow_7, \downarrow_7\rangle$ ; for the former expression, all seven of the  $f$ -electrons on both Gd atoms are spin up, and for the latter, all seven  $f$ -electrons on one Gd atom are spin up and all seven on the other Gd atom are spin down.  $|\uparrow_7, \uparrow_7\rangle$  is a spin eigenfunction ( $S = 7$ ,  $M_S = 7$ ) and  $|\uparrow_7, \downarrow_7\rangle$ , for which  $M_S = 0$ , can be expressed as a combination of pure spin states with  $S = 0, 1, \dots, 7$ . The energy of the high spin state can be identified with the energy obtained with the HDDV Hamiltonian ( $\hat{H} = -J\hat{S}_1 \cdot \hat{S}_2$ ):  $E_{|\uparrow_7, \uparrow_7\rangle} = -49/4J$ . Because overlaps between  $f$  orbitals on neighboring atoms are small,  $\langle \downarrow_7, \uparrow_7 | \uparrow_7, \downarrow_7 \rangle \approx 0$ , we can express  $|\uparrow_7, \downarrow_7\rangle$  as a combination of pure states using the Clebsch–Gordan coefficients (without overlap corrections) and obtain from that an energy expression in terms of the set of

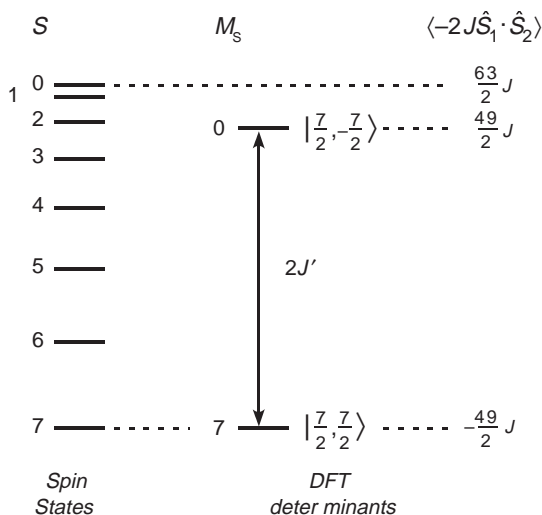


Fig. 1. Pure spin state “ladder” and determinants used in DFT for a  $Gd_2$  system ( $J, J' > 0$ ).

pure state energies,  $\{E_S\}$  [30]:

$$E_{|\uparrow_7, \downarrow_7\rangle} = \frac{3}{24} E_0 + \frac{7}{24} E_1 + \frac{7}{24} E_2 + \frac{49}{264} E_3 + \frac{7}{88} E_4 + \frac{7}{312} E_5 + \frac{1}{264} E_6 + \frac{1}{3432} E_7. \quad (4)$$

Using the HDVV Hamiltonian, we can evaluate  $E_S$  for each of the pure states ( $E_S = (J/4)(S(S+1))$ ) and substitute into this expression to obtain

$$E_{|\uparrow_7, \downarrow_7\rangle} = \frac{49}{4} J \Rightarrow \frac{49}{2} = E_{|\uparrow_7, \downarrow_7\rangle} - E_{|\uparrow_7, \uparrow_7\rangle}. \quad (5)$$

An identical value for  $E_{|\downarrow_7, \uparrow_7\rangle}$  is obtained from the expectation value,  $\langle \uparrow_7, \downarrow_7 | \hat{H} | \uparrow_7, \downarrow_7 \rangle$ , directly and this is how one can correlate computed SDFT energies with coupling parameters *in practice*; the point of this discussion is to demonstrate the equivalence of this procedure with the broken-symmetry approach (see Fig. 1).

When we refer calculated energies differences  $E_{|\uparrow_7, \uparrow_7\rangle}$  and  $E_{|\downarrow_7, \uparrow_7\rangle}$  to exchange couplings ( $J'$ ) in the Ising Hamiltonian, the “pseudo-spin” vector takes only two values,  $+1$  ( $\alpha$ ) and  $-1$  ( $\beta$ ), and as a result we obtain

$$2J' = E_{|\uparrow_7, \downarrow_7\rangle} - E_{|\uparrow_7, \uparrow_7\rangle}. \quad (6)$$

We use the Ising exchange constants below, and to make an identification to Heisenberg coupling constants, it is clear that  $J = (\frac{4}{49})J'$ .

#### 4. Computational details

The electronic structure of our model of  $Gd_2Cl_3$  (see below) was investigated by use of density functional theory (DFT) with the Becke exchange functional [31] and the Lee–Yang–Parr correlation functional [32]. All the calculations presented here were performed using the DMol3 program [33–35] from the Cerius2<sup>®</sup> suite of programs. The double numerical basis including  $d$ -polarization function, DND, was employed in DMol3

calculations for all. The size of the DND basis is comparable to Gaussian 6-31G\* basis sets, but the numerical basis set is more accurate than a Gaussian basis set of the same size because it is numerically optimized [33]. A small frozen-core ( $1s2s2p3s3p3d$ ) effective potential was used for Gd. All calculations included scalar relativistic effects and open-shell configurations.

Structural parameters for the heavy elements (Gd and Cl) were taken from the X-ray crystallographic data for the condensed cluster phase  $Gd_2Cl_3$ , as described below [36]. In constructing a 1-D model compound, phosphine oxide ligands,  $OPH_3$ , were used to “cap-off” the terminal positions of the  $Gd_4Cl_6$  chains; partial geometry optimizations for the positions of the phosphine oxides were performed using an analogous yttrium model system,  $Y_4Cl_6(OPH_3)_2$ . All calculations of competing magnetic states were conducted using a common geometry. The convergence criterion for the energy was set at  $10^{-6}$  a.u. Band calculations and quantities derived there from (energies, spin densities) were carried out using a mesh of 10  $k$ -points for all the states, except the ferromagnetic and antiferromagnetic ground spin-state patterns where 25  $k$ -points were used to obtain density-of-states (DOS) plots of higher resolution. Since all band calculations were carried out on a system with a doubled cell,  $Gd_8Cl_{12}(OPH_3)_4$ , the 10  $k$ -point mesh is equivalent to a 20  $k$ -point set for the conventional unit cell. Typical differences between spin pattern energies using a mesh of 10 and 25  $k$ -points was about 0.17%.

Recent investigations indicate that calculated  $J$  values may be overestimated using the BLYP functional [37]. As we discuss below, the origin of  $f$ – $f$  effective exchange is the local  $d$ – $f$  exchange interaction. It is therefore not clear that such concerns should apply to cases where the principal source of effective exchange is local  $d$ – $f$  interaction, if we know the accuracy with which the local  $d$ – $f$  interaction is calculated in the functional.

#### 5. Description of $Gd_2Cl_3$

$Gd_2Cl_3$  has a structure wherein linear chains of *trans*-edge-sharing metal octahedra are bridged at the apices of the metal chains and capped on triangular faces by chlorine atoms, as shown in Fig. 2 [36,38]. As pointed out in previous studies, the structure may be formally described as a condensation  $M_6X_8$  octahedral clusters to form single chains [14]. Nevertheless, the “octahedra” are quite distorted: the Gd–Gd distances on the shared edges significantly shorter (3.37 Å) than Gd–Gd distances significantly shorter (3.37 Å) than Gd–Gd distances parallel with the chain propagation axis ( $b = 3.90$  Å); Gd–Gd distances between basal and apical atoms range from 3.71 to 3.78 Å.  $Gd_2Cl_3$  is a semiconductor with band gap of  $\sim 0.85$  eV [39], as

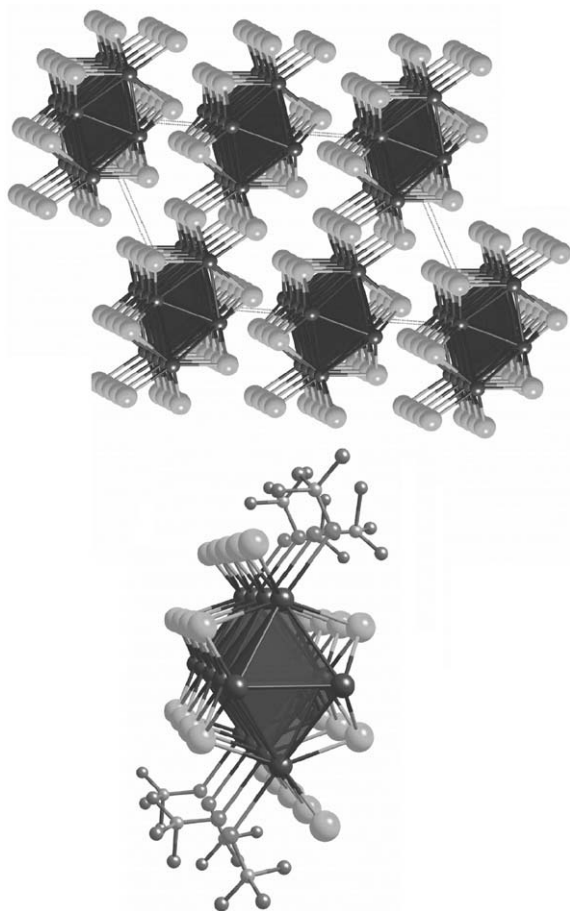


Fig. 2. Relationship between the model  $\text{Gd}_8\text{Cl}_{12}(\text{OPH}_3)_4$  and the parent  $\text{Gd}_2\text{Cl}_3$  structure.

inferred from resistivity measurements and the presence of a gap is consistent with the measured photoelectron spectrum and published electronic structural calculations [40].

Previous band structure calculations indicate that the sesquichlorides have three low-lying, overlapping occupied  $d$  bands that contain the metal–metal bonding of the shared edge and these bands split off from the remainder of the  $d$  block, giving a gap of  $\sim 0.7$  eV [41]. The semiconducting behavior is consistent with 6 metal  $d$  valence electrons per  $\text{Gd}_4\text{Cl}_6$  unit cell available for metal–metal bonding in the structure. A semilocalized bonding picture of isotypic  $\text{Y}_2\text{Cl}_3$  extracted from the band structure revealed that metal–metal bonding orbitals consist of two  $4c-2e$  bonds and one  $2c-2e$  bond per unit cell, further clarifying both the structure–property relationships of these compounds [42].

Although  $\text{Gd}_2\text{Cl}_3$  has been investigated by EPR, NMR, and magnetic susceptibility measurements [43], the results of neutron diffraction experiments on single crystals of  $\text{Gd}_2\text{Cl}_3$  provided the most detailed information concerning a 3-D antiferromagnetic phase transition at 26.8 K leading to a magnetic supercell ( $a, b, 2c$ ) [44]. Within the 1-D chains, the moments of the Gd

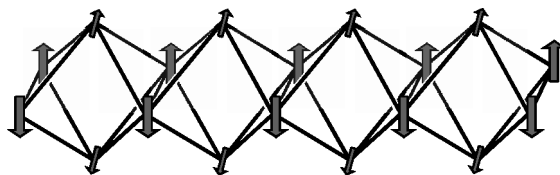


Fig. 3. Intrachain magnetic ordering according to neutron diffraction results [44]; vertices represent Gd atom positions.

atoms at the condensed octahedra sites are aligned along the chain direction, but are in an antiparallel arrangement across the short Gd–Gd bond shared by the octahedra as depicted in Fig. 3. The moments on the apex atoms do not order, as one might expect, given the geometric frustration that should occur in relation to the spin ordering from the basal atoms. Adjacent chains are coupled antiferromagnetically.

## 6. Model structure

While a study of the 3-D magnetic ordering in  $\text{Gd}_2\text{Cl}_3$  would be desirable, we have so far limited our investigation to the ordering in 1-D chain models of  $\text{Gd}_2\text{Cl}_3$ . To build a meaningful 1-D model, important considerations include preservation of the bonding character found in the chains of condensed octahedra and maintenance of the coordination environment around Gd. In the structure of  $\text{Gd}_2\text{Cl}_3$ , each metal center is coordinated to the chloride atom of two adjacent 1-D condensed chains forming a 2-D sheet, allowing for additional interactions through the basal and apical Gd–Cl–Gd bridges. However, since interactions within the chains are likely to control the 1-D magnetic structure, only those contacts will be included in our model structure. Hence, our unit cell consists of eight gadolinium atoms, 12 chloride ligands, and four phosphine oxide ligands,  $\text{OPH}_3$ , as shown in Fig. 2. Our model preserves the metal backbone of the chain and the chloride ligands that both cap the triangular side faces of the octahedra and bridge between two octahedra within the chain. Each chain was separated by a distance of 12.57 Å along the  $c$  direction and 11.87 Å along the  $a$  direction. Phosphine oxide ligands fill the coordination site provided by the apical Gd–Cl contacts lost upon separating the chains. Doubling of the unit cell in the chain direction ( $b$ ) was necessary for two reasons: (1) crowding of adjacent phosphine oxide ligands is avoided by alternating their orientation within the doubled cell; (2) necessary flexibility in calculations of alternative antiferromagnetic spin arrangements is thereby enabled. Partial geometry optimizations for the positions of the phosphine oxides were performed using an analogous yttrium model system,  $\text{Y}_4\text{Cl}_6(\text{OPH}_3)_2$ ; this resulted in Ln–O–P angles of  $38.8^\circ$  and  $120^\circ$  to prevent close H–H contacts. The closest H–H distance is 2.97 Å, well

beyond van der Waals contact. Use of neutral phosphine oxide ligands allows one to avoid unphysical charge density accumulation that would have accompanied the use of anionic ligands.

## 7. Results

### 7.1. $4f$ – $5d$ exchange in the Gd atom

Before directly considering  $\text{Gd}_2\text{Cl}_3$ , we present results using SDFT calculations on the Gd atom. Particularly relevant is a comparison between theory and experiment for the energy gap between the electronic ground state ( $^9D$ ) and the first excited state ( $^7D$ ) within the ground configuration ( $[\text{Xe}]4f^75d^16s^2$ ). Qualitatively, this calculation yields the exchange energy penalty required to flip the  $5d$ -electron spin in opposition to the  $4f^7$  spins (see Fig. 5 below). The energy difference is calculated using the two determinants,  $\Phi_{\uparrow_7,\uparrow}$  and  $\Phi_{\uparrow_7,\downarrow}$ , where the subscript notation indicates the spin of the seven  $4f$  electrons and the single  $5d$  electron separately;  $\Phi_{\uparrow_7,\uparrow}$  is a spin eigenfunction, but the spin contamination of  $\Phi_{\uparrow_7,\downarrow}$  must be accounted for.

The  $f^7d^1$  configuration yields five distinct  $^7D$  states, but four of these derive from coupling the  $d$  electron ( $^2D$ ) with sextet excited states of the  $4f^7$  core ( $^6P, ^6D, ^6F, ^6G$ ) and spectroscopic data show that such states lie very high in energy. To a good approximation then, the spin contamination of  $\Phi_{\uparrow_7,\downarrow}$  is accounted for by constructing an  $S = 3$  spin eigenfunction that is orthogonal to the  $^9D$  ground state, since it is the only other state with a  $4f^7(^8S)$  core. The components of  $^9D$  with  $M_S = 4$  and  $M_S = 3$  are

$$\begin{aligned}\Psi(^9D, 4) &= \Phi_{\uparrow_7,\uparrow}, \\ \Psi(^9D, 3) &= \sqrt{\frac{1}{8}}\Phi_{\uparrow_7,\downarrow} + \sqrt{\frac{7}{8}}\left[\frac{1}{\sqrt{7}}\sum_{i=1}^7\Phi_{\uparrow_6\downarrow i,\uparrow}\right],\end{aligned}\quad (7)$$

where the second function can be simply derived from the first by operating with a spin-lowering operator. For the orthogonal components of  $^7D$  with  $M_S = 3$ , we can write

$$\Psi(^7D, 3) \cong \sqrt{\frac{7}{8}}\Phi_{\uparrow_7,\downarrow} - \frac{1}{\sqrt{8}}\left[\frac{1}{\sqrt{7}}\sum_{i=1}^7\Phi_{\uparrow_6\downarrow i,\uparrow}\right]\quad (8)$$

which, as can be readily confirmed, is a spin eigenfunction with  $S = 3$ . From these two expressions, we obtain an expression for  $\Phi_{\uparrow_7,\downarrow}$  in terms of the pure state functions:

$$\Phi_{\uparrow_7,\downarrow} = \sqrt{\frac{7}{8}}\Psi(^7D, 3) - \sqrt{\frac{1}{8}}\Psi(^9D, 3).\quad (9)$$

Assuming this approximate relation applies, we can use the exact electronic Hamiltonian (excluding, say, spin-orbit coupling) to evaluate  $E_{\uparrow_7,\downarrow} = \langle \Phi_{\uparrow_7,\downarrow} | \mathcal{H} | \Phi_{\uparrow_7,\downarrow} \rangle$ ,

which leads to a simple expression for the energy difference between the  $^9D$  ground state and the lowest  $^7D$  excited state in terms of energies calculated with SDFT:

$$\begin{aligned}E_{\uparrow_6,\downarrow} &= \frac{7}{8}E(^7D) + \frac{1}{8}E(^9D), \\ E(^7D) - E(^9D) &= \frac{8}{7}[E_{\uparrow_7,\downarrow} - E(^9D)] = \frac{8}{7}[E_{\uparrow_7,\downarrow} - E_{\uparrow_7,\uparrow}].\end{aligned}\quad (10)$$

The calculated gap using the BLYP functional and the double numeric basis sets discussed in the computational section is  $5693\text{ cm}^{-1}$ , about 89% of the spectroscopically measured gap of  $6394\text{ cm}^{-1}$  (after averaging over spin-orbit splitting in both states) [45].

A final complication that should be mentioned arises from a well-known artifact of DFT: although both the  $^9D$  and  $^7D$  states are orbitally degenerate, the energies computed for these states with all current functionals in fact depends slightly on which  $d$  orbital is actually occupied [46]. In our case, we examined the difference of occupying one of the four spatially equivalent ‘‘cloverleaf’’ orbitals (i.e., not  $d_{z^2}$ ) in both states, and the energy difference given reflects this choice.

### 7.2. Magnetic ordering in $\text{Gd}_2\text{Cl}_3$

In order to directly assess the ability of the broken-symmetry SDFT approach to reproduce the magnetic ordering pattern observed in  $\text{Gd}_2\text{Cl}_3$ , we carried out electronic band calculations for seven competing spin patterns: one ferromagnetic, one ferrimagnetic, and five antiferromagnetic. The calculated relative energies for such patterns are shown in Fig. 4. In each case we also show the symmetry of the potential that the  $4f$  electron ‘‘cores’’ impose on the motion of the  $5d$  and other valence electrons. As we shall argue below, the origin of the differences computed in all our calculations is the  $d$ -band mixing induced by the perturbation of *intra-atomic*  $4f$ – $5d$  exchange. Since the atomic calculations underestimate the magnitude of that exchange by  $\sim 11\%$  (see above), we expect that calculated energy differences for this model are probably an underestimation of the ‘‘true’’ differences between the spin patterns.

The most important and consistent characteristic of the results in Fig. 4 is a preference for antiferromagnetic spin patterns in comparison to the ferro- or ferrimagnetically coupled spin arrangements. The lowest energy calculated pattern is in correspondence with the experimentally observed spin ordering as far as the basal atoms are concerned, i.e., antiparallel spin alignment prevails for atoms across the basal planes of the condensed octahedra. (The lack of significant magnetization on the apical atoms cannot be modeled in our calculation.) Interestingly, the second lowest calculated pattern does not reproduce the observed basal spin ordering. Indeed, all the two patterns seem to

Label, Pseudosymmetry, <sup>a</sup> Relative SDFT Energy, <sup>b</sup> Ising Energy Expression	Spin Patterns
Ferromagnetic, $D_{2h}(b)$ $1738.3 \text{ cm}^{-1}$ $-2J'_1-4J'_2-16J'_3-4J'_4$	
Ferrimagnetic, $C_{2v}(b)$ $729.2 \text{ cm}^{-1}$ $-2J'_1-4J'_2-4J'_4$	
Antiferro V, $C_s(2b)$ $458.1 \text{ cm}^{-1}$ $-2J'_1+4J'_2-4J'_4$	
Antiferro IV, $C_s(2b)$ $449.2 \text{ cm}^{-1}$ $-2J'_1+4J'_2+4J'_4$	
Antiferro III, $C_2(2b)$ $311.3 \text{ cm}^{-1}$ $+2J'_1+4J'_2+4J'_4$	
Antiferro II, $D_{2h}(b)$ $89.5 \text{ cm}^{-1}$ $-2J'_1-4J'_2+16J'_3-4J'_4$	
Antiferro I, $C_s(b)$ $0.0 \text{ cm}^{-1}$ $+2J'_1-4J'_2-4J'_4$	

<sup>a</sup>“Pseudosymmetry” refers to the highest point symmetry of the spin-dependent potential the  $4f^7$  electron moments exert on the valence electrons. Labels “ $b$ ” and “ $2b$ ” refer to the periodicity of potential along the  $b$  (chain) axis.

<sup>b</sup> Relative energy and Ising expressions are given per  $\text{Gd}_8\text{Cl}_{12}(\text{OPH}_3)_4$  cell.

Fig. 4. Seven spin patterns, energies, and Ising expressions.

have in common is their translational periodicities—both patterns have the same cell length as the structure ( $b$ ). Spin patterns in which  $4f^7$  spins alternate along the chain propagation axis (with  $2b$  periodicities) all lie higher in energy.

It is tempting to account for the marked difference in the two lowest energy patterns, Antiferro I and Antiferro II, in terms of the Ising coupling parameters that appear in the difference between the two orderings' Ising energy expressions:  $E(\text{II}) - E(\text{I}) = 4J'_1 - 16J'_3$ . If

the antiferromagnetic coupling between opposite basal atoms ( $J'_1$ ) is strong enough, then Antiferro I prevails as the ground state; if the antiferromagnetic coupling between basal and apical atoms ( $J'_3$ ) is strong enough (greater than 25% of  $J'_1$ ), then Antiferro II will prevail. Experiment favors the former interpretation, but as we shall see below, the Ising analysis runs into difficulties when one attempts to account for *all* the calculated results in Fig. 4, as we shall see in what follows.

SDFT calculations and the broken-symmetry approach have been successfully applied to the estimation of the exchange coupling constants for a variety of binuclear transition metal complexes, with good agreement between computed and experimental values [47]. From the computed results in Fig. 4, let us examine whether we can extract values for the Ising exchange parameters for this system. Under the (Ising) hypothesis of exchange interaction additivity, it is a simple matter to assign to each spin pattern an expression for the magnetic energy of each spin pattern, as shown in Fig. 4. The energy associated with any one spin pattern, A, can be written as

$$E_{\text{spin pattern A}} = - \sum_{i < j} Z_{ij} \hat{S}_{z,i} \hat{S}_{z,j} J'_{ij}, \quad (11)$$

where  $\hat{S}_{z,i}$  and  $\hat{S}_{z,j}$  are respective pseudo-spins (+1 and -1) on sites of types  $i$  and  $j$  for pattern A,  $J'_{ij}$  is the magnetic coupling constant between them, and  $Z_{i,j}$  is the number of  $i$ - $j$  neighbors. Energy differences are readily evaluated. In the present case, four magnetic constants have been considered, namely  $J'_1$ ,  $J'_2$ ,  $J'_3$ , and  $J'_4$ , as defined in Fig. 4. (To scale these values for the Heisenberg Hamiltonian, all  $J'_i$  values need to be multiplied by  $\frac{49}{4}$ .)  $J'_1$  and  $J'_2$  represent the basal-to-basal couplings across the octahedra and along the chain propagation axis, respectively.  $J'_3$  represents the exchange coupling between apical-basal atom pairs and  $J'_4$  represents the coupling between two apical atoms along the chain. Because the ferrimagnetic spin pattern gives rise to an asymmetric charge density in which structurally equivalent apical atoms have differing total charge, we dropped it from consideration in evaluating magnetic coupling constants (its inclusion does not alter the fundamental nature of our conclusions, however). Of the remaining six spin patterns, one may compute five independent energy differences from the SDFT results and each difference may be set equal to an Ising parameter expression; we therefore have five equations involving four  $J'_i$  values (Table 1). Finally, we tested the efficacy of the Ising model in fitting the SDFT results by dropping one of each of the remaining equations in turn and solving the remaining system of equations analytically. The results of this test are shown in Table 2.

One might presume that we could identify and order the pairwise coupling parameters in magnitude so that we could correlate our SDFT results. However, the  $J'_i$  values vary widely when different energy differences are used to determine the spin pattern energies and such an assessment discussing strength and, sometimes, even signs cannot be made. More importantly, after obtaining coupling constants that well represent the four energy differences, the calculated energies of the patterns not used in each case (ferrimagnetic and other dropped pattern) is poor. We conclude that the Ising model does not provide an adequate description of  $d$ -electron-

Table 1

Five possible equations used in calculating Ising coupling constants ( $J$ 's)<sup>a</sup>

$\Delta E_{\text{A-B}}$	$\sum_{i,j} Z_{i,j} J_{i,j}$	Energy difference (cm <sup>-1</sup> )
$\Delta E_{\text{Ferro-Antiferro V}}$	$-8J_2 - 16J_3$	1280
$\Delta E_{\text{Antiferro V-Antiferro IV}}$	$-8J_4$	8.9
$\Delta E_{\text{Antiferro IV-Antiferro III}}$	$-4J_1$	138
$\Delta E_{\text{Antiferro III-Antiferro II}}$	$4J_1 + 8J_2 - 16J_3 + 8J_4$	221.8
$\Delta E_{\text{Antiferro II-Antiferro I}}$	$-2J_1 + 16J_3$	89.6

<sup>a</sup> Ferrimagnetic spin pattern was not included (see text).

mediated  $f$ - $f$  exchange interactions. Assuming the broken-symmetry approach is valid for determining parameters in a Heisenberg model (i.e., that the discussion of Gd<sub>2</sub> dimers given above can be generalized to the band case), a Heisenberg model would also be inadequate. If Gd<sub>2</sub>Cl<sub>3</sub> were metallic, this would probably be expected since it is commonplace to treat metallic systems by considering the effect of exchange on electrons near the Fermi surface [48–50]. It is perhaps more surprising that these pairwise exchange models fail even for this closed shell (semiconducting) compound. Whatever the limitation of our present treatment (e.g., basis set or the use of the BLYP functional), we can reasonably assume that an improvement in theory is unlikely to produce results that revive a pairwise exchange model, with the possible exception of a model includes significant anisotropic exchange.

Previous analysis had postulated that 1-D magnetic correlations in Gd<sub>2</sub>Cl<sub>3</sub> persist at temperatures well above the 3-D ordering temperature of 26.8 K [15]. While this suggestion is intuitively appealing, our results leave us unable to comment on this speculation. As we have seen, pairwise exchange parameters are elusive and without them, the excitation energies that accompany local spin fluctuations are difficult to estimate with the results we have at hand.

### 7.3. $d$ -Electron mediated exchange

In previous work, we demonstrated that there exists a straightforward interpretation of  $d$ -electron-mediated  $f$ - $f$  exchange involving the use perturbation theory. To explain the general features of this approach, it is useful to summarize our treatment of  $[\text{Gd}_3\text{I}_6(\text{OPH}_3)_{12}]^{n+}$  ( $n = 1, 2, 3$ ), a trinuclear cluster that mimics the three-center bonding found in the ferromagnetic conductor GdI<sub>2</sub> [49,51,52]. In that study, we showed that the  $d^0$  system ( $n = 3$ ) exhibits negligible exchange coupling of the Gd  $4f^7$  moments, in the closed shell two- $d$ -electron system ( $n = 1$ ) antiferromagnetic coupling of  $4f^7$  moments was favored, and the open shell one- $d$ -electron system ( $n = 2$ ) exhibits strong ferromagnetic coupling of the  $4f^7$  moments. A perturbative molecular orbital (PMO) model explains how the  $4f^7$ - $d$  exchange perturbation of

Table 2  
Six possible solutions for Ising coupling constants ( $J'_i$  values)

$J'_i$	Omitted spin pattern					
	Antiferro IV	Antiferro V	Ferro	Antiferro II	Antiferro III	Antiferro I
$J'_1$	-228	-34	-34	-34	-228	-34
$J'_2$	-57	<sup>a</sup>	40	40	-57	-57
$J'_3$	-51	3	-3	-100	-51	-51
$J'_4$	96	<sup>a</sup>	-1	-1	-1	-1

<sup>a</sup> Undetermined values due to linear dependence of difference equations.

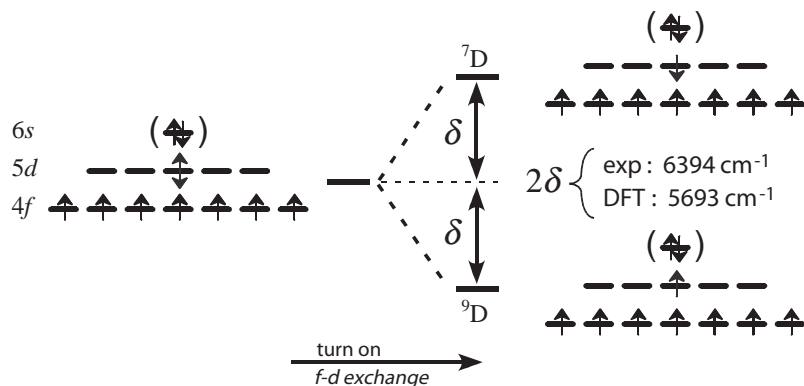


Fig. 5. Electronic splitting of Gd atom as a function of  $4f$ - $5d$  exchange perturbation.

the  $d$ -based molecular orbitals brings about these results. To describe our analysis, first consider an “unperturbed” system: a Gd atom with a  $4f^7 5d^1 6s^2$  configuration and *in the presence of an “averaged”  $4f$ - $5d$  exchange interaction* (Fig. 5). In this hypothetical situation, the  $5d$  electron experiences an average exchange field effect from the  $4f^7$  half-shell and has no preferred spin orientation. Upon applying the exchange perturbation, a  $d$ -electron with its spin aligned with (against) the  $4f^7$  moment is stabilized (destabilized) by an energy  $\delta$ .

We can treat the  $\text{Gd}_3$  trinuclear cluster model in the same spirit and adopt the simple three-center bond model shown in Fig. 6 to account for the 3 MOs of this three-center bonding system.  $\Delta$  represents the gap between the bonding orbital and the degenerate antibonding orbitals. Orbital plots clearly demonstrate that the  $d$ -electron(s) in the  $d^1$  ( $d^2$ ) systems reside in a delocalized three-center bond orbital—underlining the plausibility of this treatment. For simplicity, the MOs are assumed to be a linear combination of Gd  $d$ -orbitals with no ligand contribution or  $6s$ -hybridization taken into account.

In the all-spin-aligned “ferromagnetic” case,  $4f$ -moment ordering simply induces a first-order splitting of the  $\alpha$ - and  $\beta$ -spin molecular orbitals, and since the exchange potential felt by the  $d$  electrons maintains symmetry, no symmetry breaking occurs and no

second-order perturbation effects are limited to mixing of the occupied  $a'_1$  orbital with orbitals of the same symmetry. When one of the  $4f$ -moments is flipped antiparallel with the others (“ferrimagnetic” case), the exchange perturbation lowers the symmetry and mixing between the bonding and antibonding MOs is thereby induced, yielding a second-order stabilization of both  $\alpha$  and  $\beta$  spins (manifest in polarization of each  $d$ -spin orbital toward  $4f^7$  centers of like spin).

In summary, when one has a closed  $d$ -shell system (like the  $d^2$  trinuclear cluster), antiferromagnetic coupling is inevitably favored because antiferromagnetic  $4f^7$ -spin patterns inherently *break symmetry* and mix unoccupied orbitals into the occupied orbitals. Spatially, this allows for the stabilizing effect of spin polarization to occur. Any  $f^7$  spin ordering that is effective at inducing  $5d/6s$  spin polarization will tend to have lower energy because such spin polarization allows the delocalized electrons to spend more time in the vicinity of the like-spin  $f$ -electrons. In general, there is no reason to expect that such a mechanism of coupling should produce a spin-state energy ordering that conforms to a model built upon pairwise exchange coupling. With the two parameters,  $\delta$  and  $\Delta$ , we can achieve a satisfactory fit with the SDFT energies calculated for six different “states” (i.e., determinants) for  $[\text{Gd}_3\text{I}_6(\text{OPH}_3)_{12}]^{n+}$  ( $n = 1, 2$ ) systems [13].

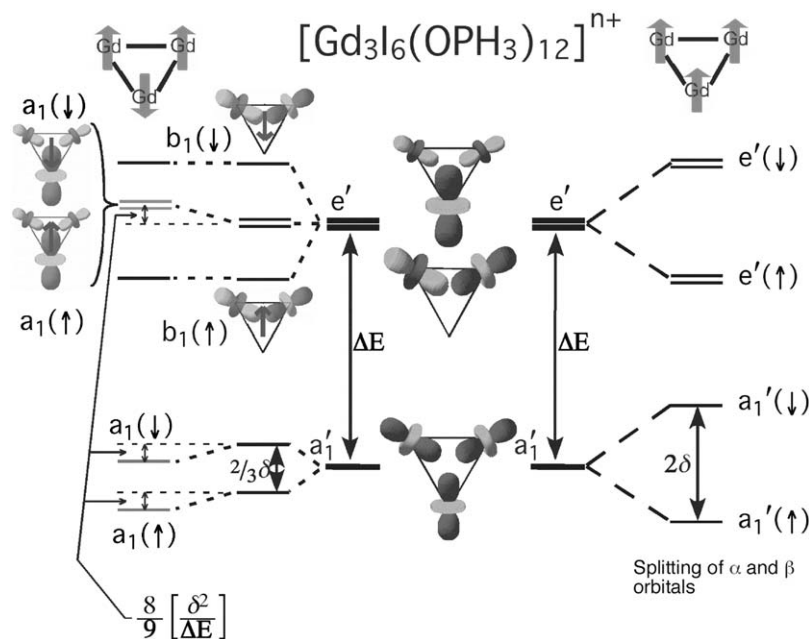


Fig. 6. Treatment of  $4f$ – $5d$  exchange interaction in model  $\text{Gd}_3\text{I}_6(\text{OPH}_3)_{12}^{n+}$  as a second-order perturbation to the system.

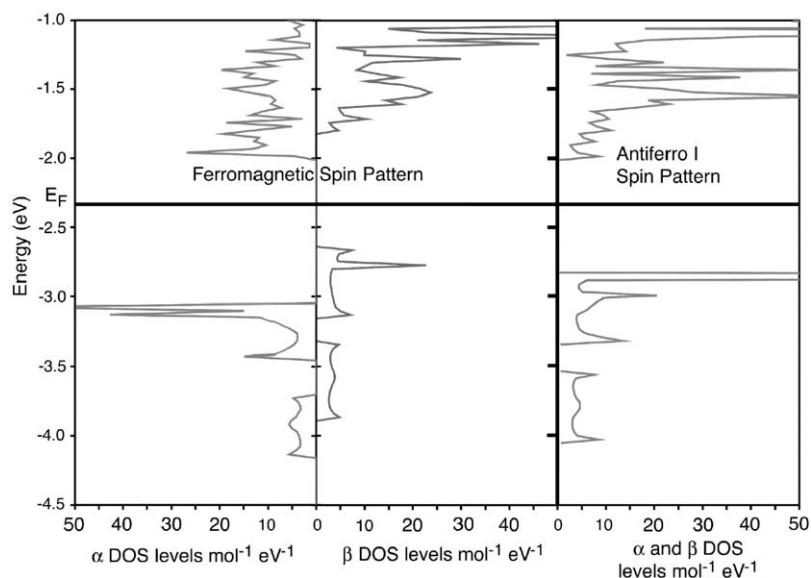


Fig. 7. DOS plots of the ferro spin pattern and antiferro I spin pattern.

In view of the foregoing discussion and the closed  $d$ -shell (semiconducting) nature of our  $\text{Gd}_4\text{Cl}_6(\text{OPH}_3)_2$  model chains (and  $\text{Gd}_2\text{Cl}_3$  itself), we should not be surprised that all the low-energy spin patterns are antiferromagnetic. We can identify features in DOS plots obtained with various  $4f^7$ -spin patterns that show how the extended chain system and trinuclear cluster are analogous; see Fig. 7. As expected, the bands in the vicinity of the Fermi level are Gd-localized. The results amplify those of previous tight-binding calculations of both  $\text{Gd}_2\text{Cl}_3$  and its yttrium analog: three doubly-occupied  $5d$  bands (per  $\text{Gd}_4\text{Cl}_6$  unit cell) are separated

by a significant gap from the rest of the low-lying unoccupied metal hybridized  $d$  and  $s$  bands [41,42,53]. The calculated gap ranges from 0.68 to 1.0 eV for different antiferromagnetic spin patterns with the gap for Antiferro I equal to 0.82 eV. This is in good agreement with the 0.85 eV band gap seen experimentally for  $\text{Gd}_2\text{Cl}_3$ . The  $\alpha$ - and  $\beta$ -DOS plots for all the antiferromagnetic cases are identical because although the  $\alpha$ - and  $\beta$ -electrons localize on different atoms, the  $\alpha$ - and  $\beta$ -spin distributions are spread over symmetry-equivalent sets of atoms. Examination of the  $\alpha$ - and  $\beta$ -DOS plots for the ferromagnetic spin pattern shows a

Table 3  
Magnitudes of summed Gd 5*d* and 6*s* spin polarizations for basal and apical atoms

Spin pattern	Spin polarization		Relative energy (cm <sup>-1</sup> )
	Basal	Apical	
Ferro	0.087	0.034	1738.2
Ferri <sup>a</sup>	0.188, 0.198	0.083, 0.355	729.2
Antiferro V	0.294	0.227	458.1
Antiferro IV	0.295	0.227	449.2
Antiferro III	0.326	0.227	335.5
Antiferro II	0.294	0.295	89.5
Antiferro I	0.417	0.235	0

All values are computed with precision within  $\pm 0.002$ .

<sup>a</sup>The ferrimagnetic spin-pattern polarizations are different on structurally equivalent atoms because the ferrimagnetic potential does not preserve chemical equivalence of symmetry-related atoms.

stabilization and destabilization of the  $\alpha$ - and  $\beta$ -electrons, respectively. Since the exchange potential felt by the *d* electrons maintains symmetry, the 4*f*<sup>7</sup>-spin patterns induce little mixing between valence and conduction band orbitals. In our qualitative perturbation analysis then, this semiconducting ferromagnetic-ordered system experiences little overall stabilization because the first-order stabilization of  $\alpha$ -spin *d* bands is cancelled by destabilization of  $\beta$ -spin *d* bands and there is little second-order stabilization. In contrast, while the antiferromagnetic alternatives experience no net first-order splitting between  $\alpha$ - and  $\beta$ -spin *d* bands, both  $\alpha$ - and  $\beta$ -spin *d* bands are stabilized in second-order by the valence-conduction band mixing induced by symmetry breaking.

While DOS plots are useful in illustrating the distinction between the ferro- and antiferromagnetic cases, we gain no further insight into the specific ordering among the antiferromagnetic alternatives. Though a specific “orbital explanation” for the calculated ordering is not apparent, it is nevertheless instructive to examine the 5*d* and 6*s* spin polarizations (i.e., the local differences in  $\alpha$ - and  $\beta$ -spin populations). These are given for all of the calculated spin patterns obtained via Mulliken population analysis (summed over all *k*-points calculated) and gathered in Table 3. On each Gd atom, for every spin pattern, the 5*d* and 6*s* spin polarizations mirror the spin orientations of 4*f*<sup>7</sup> core for that atom—hence, we have given only the polarization magnitudes in Table 3. We have combined 5*d* populations with 6*s* populations because they track with each other, though the 6*s* polarization is consistently smaller. Typically, total 5*d* populations are about 2.3–2.7 times larger than the 6*s* populations, while the polarization for 5*d* populations are 5–6 times larger than the polarizations of the 6*s* populations. (This reflects the fact that the intraatomic exchange interaction between the 4*f* electrons and the more diffuse 6*s* electrons is typically about one-third that of the 4*f*–5*d* interaction.)

The data in Table 3 are unambiguous in confirmation of our perturbation-theoretic interpretation. The symmetry-breaking antiferromagnetic patterns all induce much greater spin polarization than is seen in the ferromagnetic case. Beyond that, however, we can see that the extent of spin polarization is monotonically correlated with the relative stability of each spin pattern; the greatest spin polarization is seen in the computed ground-state pattern. One concern regarding the comparison of these results with experiment is the significance of the apical atom spin-polarizations—recall that neutron diffraction results showed no evidence of magnetic order on the apical atom positions [44]. A comparison of patterns Antiferro IV and Antiferro V is useful in this regard. These two spin orderings differ in that the apical atom 4*f*<sup>7</sup>-spins alternate in pattern IV and they remain “in-phase” in pattern V. They have similar energies, separated by only 9 cm<sup>-1</sup> per Gd<sub>8</sub>Cl<sub>12</sub>(OPH<sub>3</sub>)<sub>4</sub> unit, and they exhibit virtually identical spin-polarization magnitudes. The clear implications are that apical–basal interactions are indeed “frustrated”, even if a pairwise interaction model is not a strictly appropriate means to reveal it, and that the kind of apical–apical communication that would favor ordering is also not present.

## 8. Concluding remarks

An analysis of Gd<sub>2</sub>Cl<sub>3</sub> that correlates changes in spin densities, specific orbital contributions to DOS features, and spin-pattern variations is currently underway in our laboratory. The feasibility of extending our analysis to 3-D will also be evaluated. At this point, it seems clear that effective magnetic coupling in Gd-rich compounds is amenable to perturbative analysis of the 5*d*/6*s* electronic structure, since it is those delocalized electrons that mediate the effective *f*–*f* coupling. The nature of our approach lends itself well to considerations that are “chemical” in nature with an emphasis on orbitals and orbital interactions.

## Acknowledgments

We thank Lisa Thomson and Prof. Michael Hall for valuable help and discussions. This work is supported by the Texas Advanced Research Program (# 010366-0188-2001) and the Robert A. Welch Foundation (Grant A-1132).

## References

- [1] E. Ruiz, S. Alvarez, A. Rodriguez-Forteza, P. Alemany, Y. Pouillon, C. Massobrio, in: J.S. Miller, M. Drillon (Eds.),

- Magnetism: Molecules to Materials, Vol. II, Wiley-VCH, Weinheim, 2001, pp. 227–279.
- [2] B. Gillon, C. Mathoniere, E. Ruiz, S. Alvarez, A. Cousson, T.M. Rajendiran, O. Kahn, *J. Am. Chem. Soc.* 124 (2002) 14433–14441.
- [3] H.J. Koo, M.H. Whangbo, *J. Solid State Chem.* 151 (2000) 96–101.
- [4] H.J. Koo, M.H. Whangbo, S. Coste, S. Jobic, *J. Solid State Chem.* 156 (2001) 464–469.
- [5] M.-H. Whangbo, H.-J. Koo, D. Dai, D. Jung, *Inorg. Chem.* 41 (2002) 5575–5581.
- [6] A. Rodriguez-Fortea, P. Alemany, S. Alvarez, E. Ruiz, *Inorg. Chem.* 41 (2002) 3769–3778.
- [7] J. Tercero, C. Diaz, J. Ribas, E. Ruiz, J. Mahia, M. Maestro, *Inorg. Chem.* 41 (2002) 6780–6789.
- [8] C. Blanchet-Boiteux, J.-M. Mouesca, *J. Am. Chem. Soc.* 122 (2000) 861–869.
- [9] V. Barone, A. Bencini, D. Gatteschi, F. Totti, *Chem. Eur. J.* 8 (2002) 5019–5027.
- [10] J.B. Goodenough, in: F.A. Cotton (Ed.), *Magnetism and the Chemical Bond*, Vol. I, Interscience, New York, 1963.
- [11] P.J. Hay, J.C. Thibault, R. Hoffmann, *J. Am. Chem. Soc.* 97 (1975) 4884–4899.
- [12] O. Kahn, B. Briat, *J. Chem. Soc. Faraday Trans.* 72 (1976) 1441–1446.
- [13] L.E. Roy, T. Hughbanks, *Mater. Res. Soc. Symp. Proc.* 755 (2003), in press.
- [14] A. Simon, *Inst. Phys. Conf. Ser.* 39 (1978) 353–360.
- [15] A. Simon, H.J. Mattausch, G.J. Miller, W. Bauhofer, R.K. Kremer, in: K.A. Gschneidner, L. Eyring (Eds.), *Handbook on the Physics and Chemistry of Rare Earths*, Elsevier Science, Amsterdam, Vol. 15, 1991, pp. 191–285.
- [16] W. Heisenberg, *Z. Phys.* 49 (1928) 619–636.
- [17] P.A.M. Dirac, *Proc. R. Soc. (London) A* 123 (1929) 714–733.
- [18] J.H. Van Vleck, *The Theory of Electric and Magnetic Susceptibilities*, Clarendon, Oxford, 1932.
- [19] J.M. Dixon, J.A. Tuszyński, *Phys. Lett. A* 283 (2001) 300–308.
- [20] I.D.P.R. Moreira, F. Illas, *Phys. Rev. B: Condens. Matter* 55 (1997) 4129–4137.
- [21] F. Illas, I.D.P.R. Moreira, C. De Graaf, V. Barone, *Theor. Chem. Acc.* 104 (2000) 265–272.
- [22] L. Noodleman, *J. Chem. Phys.* 74 (1981) 5737–5743.
- [23] L. Noodleman, D.A. Case, *Adv. Inorg. Chem.* 38 (1992) 423–470.
- [24] D. Dai, M.-H. Whangbo, *J. Chem. Phys.* 118 (2003) 29–39.
- [25] A.J. Freeman, in: R.J. Elliot (Ed.), *Magnetic Properties of Rare Earth Metals*, Plenum, New York, 1972, pp. 245–334.
- [26] B.N. Harmon, A.J. Freeman, *Phys. Rev. B: Condens. Matter* 10 (1974) 1979–1993.
- [27] M.A. Ruderman, C. Kittel, *Phys. Rev. B: Condens. Matter* 96 (1954) 99.
- [28] T. Kasuya, *Prog. Theor. Phys. (Jpn.)* 16 (1956) 45.
- [29] K. Yosida, *Phys. Rev. B: Condens. Matter* 106 (1957) 893.
- [30] M. Tinkham, *Group Theory and Quantum Mechanics*, McGraw-Hill, Berkeley, CA, 1964.
- [31] A.D. Becke, *Phys. Rev. A: At. Mol. Opt. Phys.* 38 (1988) 3098–3100.
- [32] C. Lee, W. Yang, R.G. Parr, *Phys. Rev. B: Condens. Matter* 37 (1988) 785–789.
- [33] B. Delley, *J. Chem. Phys.* 92 (1990) 508–517.
- [34] B. Delley, *J. Chem. Phys.* 113 (2000) 7756–7764.
- [35] B. Delley, *Comput. Mater. Sci.* 17 (2000) 122–126.
- [36] A. Simon, N. Holzer, H. Mattausch, *Z. Anorg. Allg. Chem.* 456 (1979) 207–216.
- [37] V. Polo, E. Kraka, D. Cremer, *Theor. Chem. Acc.* 107 (2002) 291–303.
- [38] D.A. Lohken, J.D. Corbett, *Inorg. Chem.* 12 (1973) 556–559.
- [39] W. Bauhofer, J.K. Cockcroft, R.K. Kremer, H. Mattausch, C. Schwarz, A. Simon, *J. Phys. Colloq.* 8 (1988) C8-893–C8-894.
- [40] G. Ebbinghaus, A. Simon, A. Griffith, *Z. Naturforsch. A: Phys. Sci.* 37A (1982) 564–567.
- [41] D.W. Bullett, *Inorg. Chem.* 24 (1985) 3319–3323.
- [42] K.A. Yee, T. Hughbanks, *Inorg. Chem.* 31 (1992) 1620–1625.
- [43] R.K. Kremer, A. Simon, *J. Less-Common Met.* 127 (1987) 262–263.
- [44] A. Simon, *J. Alloys Compd.* 229 (1995) 158–174.
- [45] NIST, [http://physics.nist.gov/cgi-bin/AtData/main\\_asd](http://physics.nist.gov/cgi-bin/AtData/main_asd), 1999.
- [46] W. Koch, M.C. Holthausen, *A Chemist's Guide to Density Functional Theory*, Vol. 2, Wiley, New York, 2000.
- [47] E. Ruiz, P. Alemany, S. Alvarez, J. Cano, *J. Am. Chem. Soc.* 119 (1997) 1297–1303.
- [48] J. Jensen, A.R. Mackintosh, *Rare Earth Magnetism: Structures and Excitations*, Oxford University Press, Oxford, 1991.
- [49] C. Felser, K. Ahn, R.K. Kremer, R. Seshadri, A. Simon, *J. Solid State Chem.* 147 (1999) 19–25.
- [50] I. Eremin, P. Thalmeier, P. Fulde, R.K. Kremer, K. Ahn, A. Simon, *Phys. Rev. B: Condens. Matter* 64 (2001) 064425/1–064425/6.
- [51] A. Kasten, P.H. Muller, M. Schienle, *Solid State Commun.* 51 (1984) 919–921.
- [52] K. Ahn, C. Felser, R. Seshadri, R.K. Kremer, A. Simon, *J. Alloys Compd.* 303–304 (2000) 252–256.
- [53] D.W. Bullett, *Inorg. Chem.* 19 (1980) 1780–1785.

Statement of ownership, management, and circulation required by the Act of October 23, 1962, Section 4369, Title 39, United States Code: of

JOURNAL OF SOLID STATE CHEMISTRY

Published monthly except semimonthly in February and November by Elsevier Inc., 6277 Sea Harbor Drive, Orlando, FL 32887-4900. Number of issues published annually: 14. Editor: M.G. Kanatzidis, Dept. of Chemistry, Michigan State University, 320 Chemistry Building, East Lansing, MI 48824, USA.

Owned by Elsevier Inc., 525 B Street, Suite 1900, San Diego, CA 92101-4495. Known bondholders, mortgagees, and other security holders owning or holding 1 percent or more of total amount of bonds, mortgages, and other securities: None.

Paragraphs 2 and 3 include, in cases where the stockholder or security holder appears upon the books of the company as trustee or in any other fiduciary relation, the name of the person or corporation for whom such trustee is acting, also the statements in the two paragraphs show the affiant's full knowledge and belief as to the circumstances and conditions under which stockholders and security holders who do not appear upon the books of the company as trustees, hold stock and securities in a capacity other than that of a bona fide owner. Names and addresses of individuals who are stockholders of a corporation which itself is a stockholder or holder of bonds, mortgages, or other securities of the publishing corporation have been included in paragraphs 2 and 3 when the interests of such individuals are equivalent to 1 percent or more of the total amount of the stock or securities of the publishing corporation.

Total no. copies printed: average no. copies each issue during preceding 12 months: 575; single issue nearest to filing date: 575. Paid circulation (a) to term subscribers by mail, carrier delivery, or by other means: average no. copies each issue during preceding 12 months: 17; single issue nearest to filing date: 8. (b) Sales through agents, news dealers, or otherwise: average no. copies each issue during preceding 12 months: 360; single issue nearest to filing date: 325. Free distribution (a) by mail: average no. copies each issue during preceding 12 months: 86; single issue nearest to filing date: 84. (b) Outside the mail: average no. copies each issue during preceding 12 months: 9; single issue nearest to filing date: 9. Total no. of copies distributed: average no. copies each issue during preceding 12 months: 463; single issue nearest to filing date: 417. Percent paid and/or requested circulation: average percent each issue during preceding 12 months: 81.4%; single issue nearest to filing date: 79.9%.

(Signed) Paul Richmond, Manufacturing and Operations Manager